Evaluation of shear friction strength of monolithic concrete interfaces

By

: Seung-Jun Kwon, BSc, MSc, PhD, Civil & Environ. Engng., Hannam University, South Korea.

: Keun-Hyeok Yang*, BSc, MSc, PhD, Plant·Archi. Engng., Kyonggi University, South Korea.

: Yong-Ha Hwang, BSc, MSc, Archi. Engng., Kyonggi University, South Korea.

: Ashraf F. Ashour, BSc, MSc, PhD, FIStructE, School of Engng., University of Bradford, UK.

Keywords: Joint, Shear, Structural design.

Total number of words: 5053

Total number of figures: 15

Total number of tables: 3

Appendix including Tables: 1

* *Corresponding author, Department of Plant·Architectural Engineering, Kyonggi University, 154-42 Gwanggyosan-ro, Youngtong-gu, Suwon, Kyonggi-do, South Korea, Tel: +82 (0)31 249 9703, E-mail: yangkh@kgu.ac.kr*

ABSTRACT

This paper presents an integrated model for shear friction strength of monolithic concrete interfaces derived from the upper-bound theorem of concrete plasticity. The model accounts for the effects of applied axial stresses and transverse reinforcement on the shear friction action at interfacial shear cracks. Simple equations were also developed to generalize the effectiveness factor for compression, ratio of effective tensile to compressive strengths and angle of concrete friction. The reliability of the proposed model was then verified through comparisons with previous empirical equations and 103 push-off test specimens compiled from different sources in the literature.

The previous equations considerably underestimate the concrete shear transfer capacity and the underestimation is notable for the interfaces subjected to additional axial stresses. The proposed model provides superior accuracy in predicting the shear friction strength, resulting in a mean between experimental and predicted friction strengths of 0.97 and least scatter. Moreover, the proposed model has consistent trends with test results in evaluating the effect of various parameters on the shear friction strength.

Keywords: monolithic interfaces, shear friction strength, mechanism analysis, axial stress.

Introduction

The load transfer at shear interface occurred in connections between columns and corbels, squat shear walls and columns, of dapped end beams, and shear keys is governed by the shear friction action (ACI-ASCE Committee 426, 1973). The shear friction strength of concrete depends on the roughness and aggregate interlock at shear cracks developed along the interface and the magnitude of axial stresses applied to the interface. The AASHTO (2012) provision and other shear friction models (Haskett et al., 2010; Mattock, 2001; Walraven et al., 1987) indicate that the shear transfer capacity of concrete is governed by the frictional resistance including aggregate interlock and cohesion of cementititous materials along shear cracks. Hence, the shear friction capacity of

lightweight concrete (LWC) is commonly lower than that of normal-weight concrete (NWC) having the same compressive strength (Sagaseta and Vollum, 2011; Yang et al.,2012). The shear transfer capacity of reinforcing bars crossing the interfaces is also influenced by the frictional resistance of concrete as because tensile stresses in the reinforcement depends on the relative slip along the interface (Ali and White, 1999). This signifies that rupture of aggregate particles owing to crack propagation results in reducing the coefficient of friction of concrete and tensile stresses generated in the transverse reinforcement. Overall, the shear friction resistance at interfacial cracks needs to be determined considering the variation of the coefficient of friction of concrete according to the unit weight and compressive strength of concrete. However, the mechanical diversity of shear friction of different concrete types is undervalued in most of the previous models (Loov and Patnaik, 1994; Mattock, 2001; Shaikh, 1978; Walraven et al., 1987) as they are empirically formulated using limited test data with a narrow range of unit weight or compressive strength of concrete.

A few researchers (Nielsen and Hoang, 2011; Yang et al., 2012) developed numerical techniques to evaluate the shear friction capacity of concrete using the upper-bound theorem of the plasticity theory. The shear friction action of different concrete types at the interfacial shear cracks can be successfully explained using the concrete plasticity. Yang et al. (2012) demonstrated that the friction angle and cohesion of concrete can be formulated as a function of the ratio of effective tensile and compressive strengths of concrete, assuming concrete is modelled as a rigid perfectly plastic material obeying modified Coulomb failure criteria. Thus, the main objectives of the present study are:

1) To extend the approach developed by Yang et al. (2012) to account for the effects of applied axial stresses and transverse reinforcement on the shear friction action at interfacial shear cracks;

2) To produce a comprehensive database of shear friction strength of concrete measured from testing of push-off specimens of different concrete types;

3) To evaluate the reliability of the empirical equations of code provisions (AASHTO, 2012; ACI 318-14, 2014) and previous researchers (Loov and Patnaik, 1994; Mattock, 2001; Shaikh, 1978; Walraven et al., 1987) against the comprehensive database collected; and

4) To study the effect of different parameters on shear friction strength of concrete using the AASHTO equation and the proposed mechanism model, and the test results extracted from the collected database.

Mechanism analysis

Failure mechanism

The experimental investigations (Ahmed and Ansell, 2010; Hofbeck et al., 1969; Mattock and Hawkins, 1972; Yang et al., 2012) showed that a monolithic concrete interface under direct shear and axial loads is usually separated into two rigid blocks at failure, as shown in Fig. 1. The failure zone between the concrete blocks can be generally idealized as a hyperbolic yield line, as proved by Ashour and Morley (1994). One rigid block has two translational and rotational displacement components relative to the other rigid block. Thus, one rigid block can be assumed to be rotating about an instantaneous center (IC). For the idealized failure mechanism, the interfacial shear plane at failure can be regarded as a plane strain problem as lateral (out of plane) strains are prevented under the same condition of the failure section (Nielsen and Hoang, 2011; Yang et al., 2012).

Upper bound solution

The upper bound analysis uses the energy principle to calculate the shear friction strength for the kinematically admissible failure mechanism explained above. The external work (W_E) done by the applied shear (V_n) and axial loads (N_x) is:

$$W_E = V_n \omega X_{ic} - N_x \omega X_{ic} \tan\alpha \quad (1)$$

where ω is the relative rotational displacement of rigid block *I* to rigid block *II* about IC, X_{ic} is the horizontal coordinate of IC, and α is the angle between the relative displacement (δ) at the midpoint of the hyperbolic yield line chord and the failure plane chord. The sign of the external work done by N_x becomes negative as N_x has an opposite direction to the propagation of the relative displacement. For a plane strain problem, the internal energy (W_I) dissipated in concrete and transverse reinforcement along the failure surface is estimated from the following general formula (Yang et al. 2012):

$$W_I = \frac{1}{2} f_c^* \delta [l - m\sin\alpha] A_c + A_{vf} f_y \delta \cos(\theta_s - \alpha) \tag{2}$$

where $l = 1 - 2\frac{f_t^*}{f_c^*}\frac{\sin\varphi}{1-\sin\varphi}$, $m = 1 - 2\frac{f_t^*}{f_c^*}\frac{1}{1-\sin\varphi}$, f_c^* ($= \nu_c f_c^{'}$) and f_t^* ($= \nu_t f_t$) are the effective compressive and tensile strengths of concrete, respectively, ν_c and ν_t are the effectiveness factors for concrete in compression and tension, respectively, $f_c^{'}$ and f_t are the compressive and tensile strengths, respectively, of concrete, A_c is the area of failure plane, A_{vf} and f_y are area and yield strength, respectively, of the transverse reinforcement at the failure plane, θ_s is the angle of transverse reinforcement relative to the failure plane, and φ is the friction angle of concrete. The relative displacement can be also written as $\omega \cdot \left(\frac{X_{ic}}{\cos\alpha} \right)$. Applying the energy conservation principle, the shear friction strength (τ_n) of monolithic concrete interfaces can be arranged in the following form:

$$\tau_n = \frac{V_n}{A_c} = \frac{1}{2} f_c^* \frac{1}{\cos\alpha}(l - m\sin\alpha) + \rho_{vf} f_y \frac{[\cos(\theta_s - \alpha)]}{\cos\alpha} + \sigma_x \tan\alpha \tag{3}$$

where ρ_{vf} is the transverse reinforcement ratio and σ_x is the additional axial stresses normally applied to the interfaces. In accordance with the upper-bound theorem, the collapse load can be determined by considering the differential equation, $\frac{\partial \tau_n}{\partial \alpha} = 0$, which gives:

$$\alpha = \sin^{-1}\left[\frac{1}{l}\left\{m - \frac{2\left(\rho_{vf} f_y \sin\theta_s + \sigma_x\right)}{f_c^*}\right\}\right] \tag{4}$$

Effectiveness factor for compression and effective strength ratio

To transform the concrete with quasi-brittleness into an equivalent rigid perfectly plastic material obeying a modified Coulomb failure criteria, effectiveness factors are introduced and calculated by equating the area of the rigid-perfectly plastic stress-strain curve to that of the actual stress–strain curve of concrete. Hence, the values of ν_c and ν_t can be determined using the following equations (Exner, 1979):

$$\nu_c = \frac{f_c^*}{f_c^{'}} = \int_0^1 \left(\frac{\sigma_c}{f_c^{'}}\right) d\left(\frac{\varepsilon_c}{\varepsilon_u}\right) \tag{5}$$

$$\nu_t = \frac{f_t^*}{f_t} = \int_0^1 \left(\frac{\sigma_t}{f_t}\right) d\left(\frac{\varepsilon_t}{\varepsilon_{tu}}\right) \tag{6}$$

where σ_c is the compressive stress corresponding to compressive strain ε_c, ε_u is the ultimate compressive strain, σ_t is the tensile stress corresponding to tensile strain of ε_t, and ε_{tu} is the ultimate tensile strain. Yang et al. (2012) determined the effectiveness factors based on the modified versions of the compressive stress–strain relationship generalized by Thorenfeldt et al. (1987) and the tensile stress–strain relationship derived by Hordijk (1991). In this study, Yang et al.'s model (2014) was used for the compressive stress–strain relationship to cover the extensive range of unit weight (ρ_c = 1400–4000 kg/m^3) and compressive strength ($f_c^{'}$ = 10–100 MPa) of concrete. The fundamental procedure to solve Eqs. (5) and (6) was specifically explained in the previous study (Yang et al. 2012).

The effectiveness factor ν_c of concrete in compression is significantly affected by $f_c^{'}$ and ρ_c of concrete, yet independent of the maximum aggregate size (Yang et al., 2012). For concrete having $f_c^{'}$ between 20 MPa and 100 MPa and ρ_c between 1400 kg/m^3 and 4000 kg/m^3, Eq. (5) using the compressive stress–strain relationship proposed by Yang et al. (2014) and then a nonlinear multiple regression (NLMR) analysis is carried out to propose a simple equation for ν_c. Influencing parameters were combined and adjusted repeatedly by trial and error approach until a relatively higher correlation coefficient R^2 (=0.97) is achieved; as a result, the following equation for ν_c could be obtained (Fig. 2):

$$\nu_c = 0.79EXP\left[-0.03\left(\frac{f_c^{'}}{f_{co}}\right)^{0.9}\left(\frac{\rho_o}{\rho_c}\right)^{1.6}\right] \tag{7}$$

where f_{co} (= 10 MPa) and ρ_o (= 2300 kg/m^3) are the reference values for the compressive strength and unit weight, respectively, of concrete.

The effective strength ratio (f_t^* / f_c^*) required for the estimation of parameters l and m in Eqs. (3) and (4) was solved using the compressive stress–strain relationship of Yang et al. and the tensile stress–strain relationship proposed by Hordijk. From a NLMR analysis of the mathematical results obtained from Eqs. (5) and (6) against concrete having $f_c^{'}$ between 20 and 100 MPa, ρ_c between 1400 and 4000 kg/m^3 and aggregate size (d_a) between 5 and 25 mm, f_t^* / f_c^* plotted in Fig. 3 can be simply expressed in the following form:

$$\frac{f_t^*}{f_c^*} = 0.064\left[\left(\frac{f_c^{'}}{f_{c0}}\right)\left(\frac{c_0}{d_a}\right)^{1.7}\left(\frac{\rho_c}{\rho_0}\right)^{0.1}\right]^{-0.43} \tag{8}$$

where c_0 (= 25 mm) is the reference value for the maximum aggregate size.

Angle of concrete friction

Kahraman and Altindag (2004) pointed out that the concrete friction angle (φ) commonly increases with the increase of the material brittleness. In case of sliding failure of a modified Coulomb material under pure shear stress, the shear stress along the failure plane of concrete interface can be expressed as follows (Yang et al., 2012):

$$\tau_n = \frac{f_c^* \cos\varphi}{2\sqrt{k}} \tag{9}$$

where the quantity k is defined by $\frac{1+\sin\varphi}{1-\sin\varphi}$. For concrete interface without transverse reinforcement and additional axial loads, the shear friction strength can be written using Eq. (3) in the following form:

$$\tau_n = \frac{1}{2} f_c^* \frac{1}{\cos\alpha}(l - m\sin\alpha) \tag{10}$$

At failure of concrete interfaces, shear stresses obtained from Eq. (9) should be the same as that calculated from Eq. (10) and consequently φ can be obtained as below:

$$\varphi = \cos^{-1}\left(\frac{l - m\sin\alpha}{\cos\alpha}\sqrt{\frac{1+\sin\varphi}{1-\sin\varphi}}\right) \tag{11}$$

Equation (11) indicates that φ varies depending on the value of f_t^* / f_c^*. For the common values of f_t^* / f_c^* within the range between 0.01 and 0.06, the variation of φ determined from the numerical analysis of Eq. (11) is plotted in Fig. 4. Hence, φ can be proposed as a function of f_t^* / f_c^* using a simple linear regression analysis as given below:

$$\varphi = 20.65\left(\frac{f_t^*}{f_c^*}\right)^{-0.21} \tag{12}$$

Database of monolithic concrete interfaces

A total of 103 specimens providing the shear friction strength of monolithic concrete interfaces

were compiled from different experimental sources (Ahmed and Ansell, 2010; Hofbeck et al., 1969; Mattock et al., 1972, 1975 1976; Yang et al., 2012; Hwang and Yang, 2016). All compiled specimens were tested under push-off loading condition to simulate the shear friction behavior at the monolithic interfaces of two elements. As a result, all push-off specimens were reported to fail in shear friction along the interface. Appendix A lists the area of failure plane, maximum aggregate size, concrete strength and type, axial stresses, and reinforcement details at the interfacial shear plane of all push-off specimens, whereas Table 1 gives the distribution of various parameter values in the database. The concrete type according to ρ_c was classified into three groups: LWC (29 specimens) for ρ_c between 1400 and 2100 kg/m^3, NWC (71 specimens) for ρ_c between 2101 and 2500 kg/m^3, and HWC (3 specimens) for ρ_c exceeding 2500 kg/m^3. Table 1 shows that the number of HWC test specimens is very limited. Most LWC specimens were produced using artificially expanded clay granules having dry density less than 1.65 g/cm^3. HWC specimens with $f_c^{'}$ of 58.8 MPa were produced using magnetite aggregate particles with density more than 3.79 g/cm^3. The range of $f_c^{'}$ was 25.8–36.2 MPa for LWC and 16.4–62.5 MPa for NWC. Seventeen specimens had no transverse reinforcement at the interfacial shear plane. For the reinforced specimens, ρ_{vf} varied between 0.001 and 0.04, producing the transverse reinforcement capacity ($\rho_{vf}\, f_y$) varying between 1.45 MPa and 10.38 MPa. Most specimens were not subjected to additional axial stresses; only 10 and 4 specimens were under additional compressive and tensile stresses, respectively.

Comparisons of prediction models and test results

Review of existing equations

Most available equations to evaluate the shear friction capacity of concrete interfaces are based on friction action (AASHTO, 2012; ACI 318-14, 2014; Shaikh, 1978) along the interfacial shear plane or empirical equations (Loov and Patnaik, 1994; Mattock, 2001; Walraven et al., 1987)

determined from regression analysis of limited test data, as summarized in Table 2. ACI 318-14 equation ignores concrete cohesion and assumes that the applied shear force is entirely transferred by the friction action of transverse reinforcement, which is assumed to be equal to $\mu\ \rho_{vf}\ f_y$, where μ is the coefficient of friction. Hence, the frictional resistance provided by the transverse reinforcement depends on the roughness of the interfacial shear plane. For LWC interfacial shear planes, ACI 318-14 introduces a modification factor (λ) to compensate for the reduced aggregate interlock due to rupture of lightweight aggregate particles. ACI 318-14 also imposes a limiting value on τ_n as a function of concrete shear resistance to avoid overestimation of concrete interfaces with over-reinforcement or high-strength concrete. This implies that stresses in transverse reinforcement should reach its yield strength before crushing of concrete at the interface. AASHTO (2012) considers τ_n as a summation of concrete cohesion and frictional resistance of the transverse reinforcement. All transverse reinforcing bars are assumed to be perpendicularly arranged to the interface. For monolithic interface, the concrete cohesion and μ value are set at 2.76 MPa and 1.4, respectively, for NWC and 1.65 MPa and 1.0, respectively, for LWC. The concrete cohesion is regarded to be independent of $f_c^{'}$.

Shaikh (1978) proposed τ_n as a root function of the shear transfer capacity of transverse reinforcement on the basis of the regression analysis of limited test data. Walraven et al. (1987) determined the experimental parameters for shear friction using the push-off test data. The experimental parameters for NWC were generalized as a function of $f_c^{'}$. Loov and Patnaik (1994) set the μ value at 0.6 for monolithic interface and considered the effect of $f_c^{'}$ on τ_n. Loov and Patnaik limits τ_n value not to exceed 0.25 $f_c^{'}$ by comparisons with a limited test results and the proposed equation. Hence, τ_n predicted by Loov and Patnaik's equation is governed by concrete transfer capacity when ω_v is greater than 0.07 for NWC and 0.16 for all-LWC. This implies that the

concrete crushing resistance at the interface is higher for LWC than for NWC. However, the crack propagation resistance and tensile capacity of LWC are commonly lower than those of NWC having the same compressive strength (Choi et al., 2014). Mattock (2001) reviewed the effect of various parameters (including $f_c^{'}$, ρ_{vf}, and σ_x) on τ_n using push-off specimens compiled from different sources to propose alternatives to ACI equation. For the empirically developed equations for τ_n, Mattock determined the experimental constants from a regression analysis using test data with $f_c^{'}$ ranging from 17 MPa to 100 MPa. In the database, only 9 specimens were subjected to additional axial stresses. Mattock's equation also ignores the shear transfer contribution of concrete when $\rho_{vf} f_y + \sigma_x$ is less than $K_1/1.45$, where K_1 is a constant related to concrete cohesion (see Table 2). Thus, for NWC interfaces with $f_c^{'}$ less than 55 MPa and without σ_x, τ_n proportionally increases with $\rho_{vf} f_y$ when transverse reinforcement index ($\omega_v = \rho_{vf} f_y / f_c^{'}$) does not exceed 0.069.

All of the previous equations given in Table 2 commonly consider the shear transfer of transverse reinforcement as a primary mechanism of shear frictional resistance at the interfacial shear planes. For over-reinforced interfaces, the upper limit is applied in terms of the maximum crushing resistance of concrete. This implies that τ_n remains constant when $\rho_{vf} f_y$ exceeds a certain limit. Walraven et al. (1987) does not account for the reduced shear transfer capacity of LWC. The equations proposed by AASHTO provision (2012) and Mattock (2001) assume that the contribution of σ_x to τ_n is equal to that of $\rho_{vf} f_y$, although this equivalent contribution is invalid for the interface subjected to additional tensile stresses.

Comparisons with test results

Figure 5 shows comparison between the measured shear friction capacities of the push-off specimens in the database and those predicted by the proposed mechanism model and previous equations summarized in Table 2. The statistical values for mean (γ_m), standard deviation (γ_s), and

coefficient of variation (γ_v) of the ratios [$\gamma = (\tau_n)_{Exp.}/(\tau_n)_{Pre.}$] between experimental and predicted shear friction capacities are also compared in Table 3 for different groups divided according to concrete unit weight and existence of transverse reinforcement and additional axial stresses. The value of μ for HWC in the previous equations was assumed to be the same as the value specified for NWC. The specimens without transverse reinforcement were excluded from the comparisons using the equations of ACI 318-14, Shaikh, and Walraven et al. as these equations neglect the shear transfer capacity of concrete cohesion. It is to be noted that values of the ratio ($\gamma = (\tau_n)_{Exp.}/(\tau_n)_{Pre.}$) below 1.0 indicates unsafe prediction of the shear friction strength, whereas values of γ exceeding 1.0 shows a safe prediction of the shear friction strength. Important findings emerged from the comparisons are discussed below.

ACI 318-14 equation considerably underestimates the shear friction capacity of concrete interface with transverse reinforcement (Fig. 5 a) because the concrete cohesion is not considered and the shear transfer capacity of transverse reinforcement is limited by an upper bound when ω_v is more than 0.14 for normal-strength NWC and 0.19 for normal-strength all-LWC. AASHTO equation also gives an underestimation results (Fig. 5 b), regardless of the type of concrete, yet the conservatism is lower than that determined from ACI 318-14 equation. This underestimation tends to increase with the increase in concrete unit weight and compressive axial stresses. The unsafety of AASHTO equation is also observed for NWC specimens with $\rho_{vf} f_y$ less than 8 MPa. The equations proposed by Shaikh (Fig. 5 c) and Loov and Patnaik (Fig. 5 d) have similar results for specimens with transverse reinforcement. The equation of Loov and Patnaik considerably underestimates the shear transfer capacity of concrete, which results in very high values of γ_m for specimens without transverse reinforcement. Walraven's equation (Fig. 5 e) gives lower values of γ_s and γ_v than the other previous equations, revealing a narrow scatter, although the reduced aggregate interlock is not considered for LWC. However, the values of γ_m and γ_s determined from Walraven's equation

sharply increase for NWC specimens subjected to additional axial stresses. Mattock's equation (Fig. 5 f) for the specimens with transverse reinforcement has the values of γ_m and γ_s close to the equations of Shaikh and Loov and Patnaik, whereas Mattock's equation has more accuracy for specimens with additional axial stresses than such equations. This is because the regression analysis conducted by Mattock involves push-off specimens subjected to the constant axial stresses. The γ value of Mattock's equation tends to slightly decrease with the increase in $\rho_{vf} f_y$.

In summary, the preceding comparisons reveal the following limitations of the previous empirical equations: 1) The shear transfer capacity by concrete cohesion along the interface is considerably underestimated; 2) The underestimation increases for the interface subjected to additional axial stresses; 3) The accuracy is sensitive to concrete unit weight, resulting in large deviations for LWC; and 4) The inclination of transverse reinforcement to the interface is not considered in the equations formulated from the regression analysis using test data.

On the other hand, the predictions from the model proposed in this study are in better agreement with test results, regardless of the concrete unit weight and the amount of transverse reinforcement (Fig. 5 g). The overall values of 0.97 and 0.17 for γ_m and γ_s, respectively, are the lowest. Moreover, the proposed model has the best accuracy for specimens with additional axial stresses. The cohesion and coefficient of friction of concrete with different unit weights and compressive strengths can be evaluated using the equations derived from the proposed mechanism analysis. Ultimately, the proposed model provides superior accuracy in predicting the shear frictional capacity of the interfaces constructed using various concretes.

Verification of primary influencing parameters

The influence of primary parameters on τ_n of the interfaces is studied using the proposed model and AASHTO equation as well as appropriate experimental results available in the database. To examine whether the code provisions reasonably consider influencing parameters, AASHTO

equation having lower γ_s values than ACI 318-14 equation is selected. In the parametric study, one parameter is incrementally changed, while others are kept constant. However as test results in the database are collected from different sources, it would not be possible to strictly achieve this and average values of concrete and steel reinforcement properties are used.

Figure. 6 (a) shows the effect of $f_c^{'}$ on τ_n of the NWC interfaces without additional axial stresses. For the interfaces without transverse reinforcement, AASHTO equation has a constant value of 2.76 MPa for NWC and 1.65 MPa for LWC, regardless of the variation of $f_c^{'}$, indicating that the concrete cohesion is independent of $f_c^{'}$. For the interfaces with transverse reinforcement, τ_n of AASHTO equation increases up to a certain limit, beyond which it remains constant. The value of τ_n depends on $f_c^{'}$ when τ_n is governed by the upper limit of $0.25 f_c^{'}$. The kink point of τ_n against $f_c^{'}$ varies according to the value of $\rho_{vf} f_y$. AASHTO equation underestimates the shear transfer capacity by concrete cohesion. Meanwhile, τ_n predicted from the proposed model increases with the increase in $f_c^{'}$, showing a greater slope of increasing rate for the interfaces with transverse reinforcement as also demonstrated by test results.

The effect of ω_v on τ_n of NWC interfaces without additional axial stresses is shown in Fig. 6 (b). The value of τ_n determined from AASHTO equation increases with the increase of ω_v up to a certain limit, beyond which τ_n remains constant as the shear transfer capacity of over-reinforced interfaces is regarded to be governed by concrete crushing. The underestimation of AASHTO equation of experimental results becomes notable when ω_v exceeds approximately 0.1 because of the upper limit. On the other hand, the predictions obtained from the proposed model increases with the increase in ω_v, indicating that the increasing rate is gradually alleviated. For over-reinforced interfaces, the proposed model shows a better accuracy compared with experimental results.

The effect of ρ_c on τ_n of the interfaces without additional axial stresses is shown in Fig. 6 (c). AASHTO equation does not differentiate between NWC and HWC and applies the same constants for concrete having ρ_c > 2100 kg/m^3. However, the aggregate interlock capacity and tensile resistance decrease with the decrease in ρ_c (Choi et al., 2014). This implies that the experimental constants for concrete shear capacity needs to be formulated as a function of ρ_c or further subdivided according to ρ_c. The underestimation of AASHTO equation is more notable for LWC than for NWC. Test results showed that a slightly higher τ_n is observed for NWC interfaces than for LWC interfaces. The predictions obtained from the proposed model slightly increases as ρ_c increases, indicating that the slope of the increasing rate is independent of the amount of transverse reinforcement. There is no available data in the database for the various concrete unit weight subjected to additional axial stresses. According to the proposed model, the increasing rate in τ_n with ρ_c is independent of the applied axial stresses.

The effect of σ_x on τ_n of NWC interfaces with $f_c^{'}$ of 30 MPa is shown in Fig. 6 (d). For AASHTO equation, a trend similar to the relationship of ω_v and τ_n is observed, namely, further increase of τ_n is not expected for the interface without transverse reinforcement when $\sigma_x / f_c^{'}$ is more than 0.125. The threshold point of $\sigma_x / f_c^{'}$ decreases with the increase in ω_v. The predictions obtained from the proposed model increase as σ_x increases, indicating a lower slope of the increasing rate for the interfaces with transverse reinforcement.

Conclusions

An integrated model of monolithic concrete interfaces derived from the upper-bound theorem of concrete plasticity has been developed. The model is an extension to that presented in a previous investigation (Yang et al. 2012) by considering the effects of applied axial stresses and transverse

reinforcement. The angle of friction varying with concrete brittleness has been expressed as a function of the effective strength ratio of f_t^* / f_c^*. The reliability and limitation of the previous empirical equations including code provisions are examined through the comparisons with 103 push-off specimens compiled from different sources. The effect of various parameters on the shear friction strength of interfacial shear planes is also investigated using test results and prediction models of AASHTO and the present study. The following conclusions may be drawn:

1. The previous equations considerably underestimate the shear transfer capacity of concrete interfaces, especially those subjected to additional axial stresses. Furthermore, the accuracy of the previous equations exhibited high sensitivity to concrete unit weight, resulting in large deviations for lightweight concrete interfaces.
2. The proposed model provides superior accuracy in predicting the shear frictional capacity of interfaces constructed using various concretes, as indicated by the mean and standard deviation of the ratio between experimental and predicted shear frictional capacities of 0.97 and 0.17, respectively.
3. The shear friction strength increases with the increase in concrete compressive strength. However, the increasing rate of shear friction strength is slightly larger for interfaces with transverse reinforcement and without axial loads.
4. As the transverse reinforcement index increases, the shear friction strength increases. However, the increasing rate is gradually alleviated towards an upper limit of the shear friction strength.
5. A slightly higher shear friction strength is observed for NWC than LWC interfaces.
6. According to the proposed model, the shear friction strength increases as axial compressive stresses increase, indicating a lower increasing rate for interfaces with transverse reinforcement.

Acknowledgments

This work was sponsored by the National Research Foundation of Korea (NRF) grant funded by the Korea government (MSIP) (No. NRF-2014R1A2A2A09054557).

NOTATION

A_c = section area of shear failure plane

A_{vf} = area of transverse reinforcement across shear failure plane

c_0 = reference aggregate size (= 25 mm)

d_a = maximum size of aggregate

$f_c^{'}$ = concrete compressive strength

f_{co} = reference concrete compressive strength (= 10 MPa)

f_c^* = effective compressive strength of concrete

f_t = concrete tensile strength

f_t^* = effective tensile strength of concrete

f_y = yield strength of transverse reinforcement

N_x = axial load normally applied to the shear plane of concrete interface

V_n = shear force in shear plane of concrete interface

W_E = external work done by applied load

W_I = internal energy dissipated along failure plane

X_{ic} = horizontal coordinate of IC

α = angle between the relative displacement at the chord midpoint and failure plane

α_f = angle between transverse reinforcement and shear plane

γ = ratio between test results and predictions

γ_m = mean of γ values

γ_s = standard deviation of γ values

γ_v = coefficient of variation of γ values

δ = relative displacement

ε_u = ultimate strain of concrete in compression

ε_{tu} = ultimate strain of concrete in tension

θ_s = angle of transverse reinforcement relative to the failure plane

λ = modification factor for lightweight concrete

μ = coefficient of friction

ν_c = effectiveness factor for concrete compressive strength

ν_t = effectiveness factor for concrete tensile strength

ρ_c = unit weight of concrete

ρ_o = reference unit weight of concrete (= 2300 kg/m^3)

ρ_{vf} = transverse reinforcement ratio

σ_x = axial stress normally applied to the shear plane

τ_n = shear friction strength in shear plane

φ = friction angle of concrete

ω = relative rotational displacement of rigid block *I* to rigid block *II* about IC.

ω_v = transverse reinforcement index

Reference

AASHTO (2012) AASHTO LRFD bridge design specifications. *American Association of State Highway and Transportation Officials*, Washington DC, USA.

ACI-ASCE Committee 426 (1973) The shear strength of reinforced concrete members. *Journal of Structural Divisions* ***ASCE*** **99(ST 6)**: 1091–1187.

ACI Committee 318 (2014) Building code requirements for structural concrete and commentary ACI 318-14. *American Concrete Institute*, Farmington Hills, USA.

Ahmed L and Ansell A (2010) Direct shear strength of high-strength fibre concrete. *Magazine of Concrete Research* **62(5)**: 379–390.

Ali MA and White RN (1999) Enhanced contact model for shear friction of normal and high-strength concrete. *ACI Structural Journal* **96(3)**: 348–360.

Ashour AF and Morley CT (1994) The numerical determination of shear failure mechanisms in reinforced concrete beams. *The Structural Engineer* **72(23, 24)**: 395–400.

Choi SJ, Yang KH, Sim JI and Choi BJ (2014) Direct tensile strength of lightweight concrete with different specimen depths and aggregate sizes. *Construction and Building Materials* **63**: 132–141.

Exner H (1979) On the effectiveness factor in plastic analysis of concrete. Plasticity in reinforced concrete (Reports of the Working Commission). *International Association of Bridge and Structural Engineering*, Zurich, Switzerland.

Haskett M, Oehlers DJ, Mohamed Ali MS and Sharmat SK (2010) The shear friction aggregate interlock resistance across sliding planes in concrete, *Magazine of Concrete Research* **62(12)**: 907–924.

Hwang YH and Yang KH (2016) Effect of transverse reinforcement and compressive stresses on the shear friction strength of concrete. *Journal of Korea Concrete Institute* **27(4)**:

Hofbeck JA, Ibrahim IO and Mattock AH (1969) Shear transfer in reinforced concrete. *ACI Structural Journal* **66(2)**: 119–128.

Hordijk DA (1991) Local approach to fatigue of concrete. Doctor Dissertation, *Delft University of Technology*, Netherlands.

Kahraman S and Altindag R (2004) A brittleness index to estimate fracture toughness. *International Journal of Rock Mechanics and Mining Sciences* **41**: 343-348.

Loov RE and Patnaik AK (1994) Horizontal shear strength of composite concrete beams with a rough interface. *PCI Journal* **39(1)**: 48–69.

Mattock AH (2001) Shear friction and high-strength concrete. *ACI Structural Journal* **98**(1): 50–59.

Mattock AH (1976) Shear transfer under monotonic loading: A cross an interface between concrete cast at different times, *Report No. SM76–3, University of Washington*, Seattel, Washington, 1–35.

Mattock AH and Hawkins NM (1972) Shear transfer in reinforced concrete: Recent research. *PCI Journal* **17(2)**: 76–93.

Mattock AH, Li WK and Wang TC (1976) Shear transfer in lightweight reinforced concrete. *PCI Journal* **32(1)**: 20–39.

Nielsen MP and Hoang LC (2011) Limit analysis and concrete plasticity. *Prentice-Hall*, England.

Sagaseta J and Vollum RL (2011) Influence of aggregate fracture on shear transfer through cracks in reinforced concrete, *Magazine of Concrete Research* **63(2)**: 119–137.

Shaikh AF (1978) Proposed revisions to shear-friction provisions. *PCI Journal* **23**(2): 127–21.

Thorenfeldt E, Tomaszewicz A and Jensen JJ (1987) Mechanical properties of high strength concrete and application to design. *Proceeding Symposium, Utilization of High-Strength Concrete*: 149-159.

Walraven JC, Frenay J and Pruijssers A (1987) Influence of concrete strength and load history on the shear friction capacity of concrete members. *PCI Journal* **32(1)**: 66–84.

Yang KH, Sim JI, Kang JH and Ashour AF (2012) Shear capacity of monolithic concrete joints without transverse reinforcement. *Magazine of Concrete Research* **64(9)**: 767–779.

Yang KH, Mun JH, Cho MS and Kang THK (2014) A stress–strain model for various unconfined concrete in compression. *ACI Structural Journal* **111(4)**: 819–826.

TABLES AND FIGURES

List of Tables:

List of Figures:

Table 1–Incidence of various parameter values in the database.

A_c (mm^2)	Type of Concrete	Distribution					
		20000–25000	25000–30000	30000–35000	35000–40000	40000–50000	50000–60000
	LWC	8	-	21	-	-	-
	NWC	4	-	56	-	5	6
	HWC	-	-	3	-	-	-
$f_c^{'}$ (MPa)	Type of Concrete	Distribution					
		10–20	20–30	30–40	40–50	50–60	60–70
	LWC	-	21	8	-	-	-
	NWC	4	46	5	10	-	6
	HWC	-	-	-	-	3	-
ρ_{vf}	Type of Concrete	Distribution					
		0	0.001–0.01	0.01–0.02	0.02–0.03	0.03–0.04	-
	LWC	11	6	6	6	-	-
	NWC	9	23	25	11	3	-
	HWC	1	2	-	-	-	-
ω_v $(=\frac{\rho_{vf} f_y}{f_c^{'}})$	Type of Concrete	Distribution					
		0	0.01–0.05	0.05–0.10	0.10–0.15	0.15–0.25	0.25–0.35
	LWC	11	-	3	3	6	6
	NWC	9	2	13	12	18	17
	HWC	1	-	2	-	-	-
σ_x (MPa)	Type of Concrete	Distribution					
		15–10	10–5	5–0	0	0–(-5)	-
	LWC	-	-	-	29	-	-
	NWC	3	3	4	57	4	-
	HWC	-	-	-	3	-	-
$\frac{\sigma_x}{f_c^{'}}$	Type of Concrete	Distribution					
		0.3–0.2	0.2–0.1	0.1–0	0	0–(-0.1)	-
	LWC	-	-	-	29	-	-
	NWC	3	7	-	57	4	-
	HWC	-	-	-	3	-	-

Table 2–Summary of previous equations and proposed mechanism models.

Proposer	Shear friction capacity of concrete interfaces
ACI 318-11 (2011)	$\tau_n = V_n / A_v = \rho_{vf} f_y (\mu\lambda \sin\theta_s + \cos\theta_s)$; μ = 1.4 for the monolithic cast; $\tau_n \le \min\left[0.2 f_c^{'}, (3.3 + 0.08 f_c^{'})\right]$ for NWC with $\lambda = 1.0$; $\tau_n \le \min(0.2 f_{ck}, 5.5)$ for sand-LWC with $\lambda = 0.85$ and all-LWC with $\lambda = 0.75$.
AASHTO-LRFD (2012)	$\tau_n = c + \mu(\rho_{vf} f_y + \sigma_x) \le \min(0.25 f_c^{'}, T_2)$; c = 2.76 MPa, μ = 1.4, and T_2 =10.34 MPa for NWC; c = 1.65 MPa, μ = 1.0, and T_2 =6.89 MPa for LWC.
Shaikh (1978)	$\tau_n = 3.12\lambda\sqrt{\rho_{vf} f_y}$; $\lambda = 1.0$ for NWC, 0.85 for sand-LWC, and 0.75 for all-LWC.
Walraven et al. (1987)	$\tau_n = C_1 (\rho_{vf} f_y)^{C_2}$; $C_1 = 0.822 (f_c^{'}/0.85)^{0.406}$ and $C_2 = 0.159 (f_c^{'}/0.85)^{0.303}$.
Loov and Patnaik (1994)	$\tau_n = 0.6\lambda\sqrt{(0.1 + \rho_{vf} f_y) f_{ck}} \le 0.25 f_{ck}$; $\lambda = 1.0$ for NWC, 0.85 for sand-LWC, and 0.75 for all-LWC.
Mattock (2001)	$\tau_n = K_1 + 0.8(\rho_{vf} f_y + \sigma_x) \le \min(K_2 f_c^{'}, K_3)$ for $\rho_{vf} f_y + \sigma_x \ge K_1 / 1.45$; $\tau_n = 2.25(\rho_{vf} f_y + \sigma_x)$ for $\rho_{vf} f_y + \sigma_x \le K_1 / 1.45$; $K_1 = 0.1 f_c^{'} \le 5.5$ MPa, $K_2 = 0.3$, and $K_3 = 16.5$ MPa for NWC; $K_1 = 1.7$ for sand-LWC and 1.4 for all-LWC; $K_2 = 0.2$ and $K_3 = 8.3$ MPa for LWC.
This study	$\tau_n = \frac{1}{2} f_c^* \frac{1}{\cos\alpha}(l - m\sin\alpha) + \rho_{vf} f_y \frac{\cos(\theta_s - \alpha)}{\cos\alpha} + \sigma_x \tan\alpha$; $l = 1 - 2\frac{f_t^*}{f_c^*}\frac{\sin\varphi}{1-\sin\varphi}$, $m = 1 - 2\frac{f_t^*}{f_c^*}\frac{1}{1-\sin\varphi}$, $\varphi = 20.65\left(\frac{f_t^*}{f_c^*}\right)^{-0.21}$, $\frac{f_t^*}{f_c^*} = 0.064\left[\left(\frac{f_c^{'}}{f_{co}}\right)\left(\frac{c_0}{d_a}\right)^{1.7}\left(\frac{\rho_c}{\rho_0}\right)^{0.1}\right]^{-0.43}$, $\alpha = \sin^{-1}\left[\frac{1}{l}\left(m - \frac{2(\rho_{vf} f_y \sin\theta_s + \sigma_x)}{f_c^*}\right)\right]$, and $\nu_c = 0.79\mathrm{EXP}\left[-0.03\left(\frac{f_c^{'}}{f_{co}}\right)^{0.9}\left(\frac{\rho_0}{\rho_c}\right)^{1.6}\right]$.

Table 3–Comparisons of statistical values obtained from $\gamma\left[=(\tau_n)_{Exp.}/(\tau_n)_{Pre.}\right]$ values of each model.

Concrete Type	Division by σ_x (MPa) and ρ_{vf}	Statistical value	Proposer						
			ACI 318-14	AASHTO	Shaikh	Walraven et al.	Loov and Patnaik	Mattock	This study
LWC	$\sigma_x = 0$ $\rho_{vf} = 0$	γ_m	-	1.73	-	-	3.38	-	0.98
		γ_s	-	0.40	-	-	0.98	-	0.24
	$\sigma_x = 0$ $\rho_{vf} > 0$	γ_m	1.80	1.27	1.36	1.03	1.34	1.34	0.92
		γ_s	0.67	0.21	0.23	0.14	0.19	0.34	0.06
	Subtotal	γ_m	1.80	1.44	1.36	1.03	2.12	1.34	0.95
		γ_s	0.67	0.37	0.23	0.14	1.18	0.34	0.15
		γ_v	0.37	0.26	0.17	0.14	0.56	0.25	0.16
NWC	$\sigma_x = 0$ $\rho_{vf} = 0$	γ_m	-	1.27	-	-	3.17	-	1.00
		γ_s	-	0.46	-	-	0.78	-	0.17
	$-3 \le \sigma_x \le 12$ $\rho_{vf} = 0$	γ_m	-	1.51	-	-	10.94	1.51	1.17
		γ_s	-	0.35	-	-	0.29	0.35	0.29
	$\sigma_x = 0$ $\rho_{vf} > 0$	γ_m	1.68	1.13	1.13	1.06	1.18	1.15	0.92
		γ_s	0.52	0.21	0.26	0.15	0.17	0.20	0.13
	$-3 \le \sigma_x \le 12$ $\rho_{vf} > 0$	γ_m	3.25	1.64	1.99	1.76	1.85	1.50	1.14
		γ_s	2.28	0.43	1.33	0.75	0.77	0.22	0.20
	Subtotal	γ_m	2.03	1.25	1.33	1.21	1.61	1.25	0.97
		γ_s	1.27	0.34	0.72	0.45	1.72	0.27	0.17
		γ_v	0.62	0.27	0.54	0.37	1.07	0.22	0.18
HWC	$\sigma_x = 0$ $\rho_{vf} > 0$	γ_m	3.52	1.81	0.87	1.65	1.75	1.82	0.98
		γ_s	1.60	0.25	0.17	0.43	0.38	0.32	0.24
Total		γ_m	**1.98**	**1.33**	**1.34**	**1.17**	**1.90**	**1.27**	**0.97**
		γ_s	**1.16**	**0.41**	**0.64**	**0.41**	**1.63**	**0.29**	**0.17**
		γ_v	**0.59**	**0.31**	**0.48**	**0.35**	**0.86**	**0.23**	**0.17**

Appendix A

Table A-1 summarizes test data of 103 push-off specimens and predicted shear friction strengths. The predictions obtained from the previous equations of ACI 318-11, AASHTO, Shaikh, Walraven et al., Loov and Patnaik, and Mattock are given in the columns stated as (2), (3), (4), (5), (6), and (7), respectively, and the prediction using present model is given in the column (8). The ratios between measured shear friction strength and predictions using the reviewed models are also given in the table. Definitions of different parameters used in the table are explained in the notation section.

Table A-1. Basic data of existing specimens and comparison of predicted and measured shear friction strengths.

Researcher	Specimen	Concrete type	A_c (mm^2)	d_a (mm)	f_c' (MPa)	$\rho_{vf} f_y$ (MPa)	σ_x (MPa)	τ_n								$(\tau_n)_{Exp}/(\tau_n)_{Pre}$						
								Exp. (1)	Prediction							(1)/(2)	(1)/(3)	(1)/(4)	(1)/(5)	(1)/(6)	(1)/(7)	(1)/(8)
									(2)	(3)	(4)	(5)	(6)	(7)	(8)							
Hofbeck et al. (1969)	1.0	NWC	32258	22	27.8	0.0000	0	3.31	0.00	2.76	0.00	0.00	1.00	0.00	3.59	-	1.20	-	-	3.30	-	0.92
	1.1A	NWC	32258	22	27.0	1.5344	0	5.17	2.15	4.90	3.85	4.06	3.99	3.45	5.80	2.41	1.05	1.34	1.27	1.30	1.50	0.89
	1.1B	NWC	32258	22	23.0	1.4527	0	5.82	2.03	4.79	3.75	3.69	3.59	3.27	5.16	2.86	1.21	1.55	1.58	1.62	1.78	1.13
	1.2A	NWC	32258	22	26.5	3.0688	0	6.89	4.30	6.61	5.44	5.50	5.49	5.10	7.00	1.60	1.04	1.27	1.25	1.25	1.35	0.98
	1.2B	NWC	32258	22	28.8	2.9054	0	6.75	4.07	6.82	5.30	5.63	5.58	5.20	7.28	1.66	0.99	1.27	1.20	1.21	1.30	0.93
	1.3A	NWC	32258	22	26.5	4.6032	0	7.58	5.29	6.61	6.67	6.61	6.61	6.33	7.77	1.43	1.15	1.14	1.15	1.15	1.20	0.98
	1.3B	NWC	32258	22	27.0	4.3580	0	7.37	5.40	6.75	6.49	6.53	6.58	6.19	7.79	1.36	1.09	1.14	1.13	1.12	1.19	0.95
	1.4A	NWC	32258	22	31.1	6.1376	0	9.37	5.79	7.77	7.70	8.36	7.77	8.02	9.31	1.62	1.21	1.22	1.12	1.21	1.17	1.01
	1.4B	NWC	32258	22	26.6	5.8107	0	8.61	5.31	6.64	7.49	7.35	6.64	7.30	8.15	1.62	1.30	1.15	1.17	1.30	1.18	1.06
	1.5A	NWC	32258	22	31.1	7.6720	0	9.65	5.79	7.77	8.61	9.29	7.77	9.24	9.64	1.67	1.24	1.12	1.04	1.24	1.04	1.00
	1.5B	NWC	32258	22	28.0	7.2634	0	9.54	5.54	7.00	8.38	8.43	7.00	8.40	8.76	1.72	1.36	1.14	1.13	1.36	1.13	1.09
	1.6A	NWC	32258	22	29.7	9.2064	0	9.87	5.68	7.42	9.43	9.80	7.42	8.91	9.27	1.74	1.33	1.05	1.01	1.33	1.11	1.06
	1.6B	NWC	32258	22	27.9	8.7161	0	9.78	5.53	6.98	9.18	9.14	6.98	8.37	8.73	1.77	1.40	1.07	1.07	1.40	1.17	1.12
	2.1	NWC	32258	22	21.4	1.5344	0	4.07	2.15	4.90	3.85	3.65	3.55	3.36	4.99	1.89	0.83	1.06	1.11	1.15	1.21	0.82
	2.2	NWC	32258	22	21.4	3.0688	0	4.69	4.27	5.34	5.44	4.89	4.94	4.59	6.04	1.10	0.88	0.86	0.96	0.95	1.02	0.78
	2.3	NWC	32258	22	26.9	4.6032	0	5.79	5.37	6.72	6.67	6.67	6.72	6.37	7.86	1.08	0.86	0.87	0.87	0.86	0.91	0.74
	2.4	NWC	32258	22	26.9	6.1376	0	6.89	5.37	6.72	7.70	7.60	6.72	7.60	8.30	1.28	1.03	0.89	0.91	1.03	0.91	0.83
	2.5	NWC	32258	22	28.8	7.6720	0	8.96	5.60	7.20	8.61	8.81	7.20	8.64	9.01	1.60	1.24	1.04	1.02	1.24	1.04	0.99
	2.6	NWC	32258	22	28.8	9.2064	0	9.54	5.60	7.20	9.43	9.59	7.20	8.64	8.98	1.70	1.33	1.01	1.00	1.33	1.10	1.06
	3.2	NWC	32258	22	27.6	1.5603	0	3.58	2.18	4.94	3.88	4.14	4.06	3.51	5.91	1.64	0.73	0.92	0.87	0.88	1.02	0.61

	3.3	NWC	32258	22	21.4	3.0688	0	4.69	4.27	5.34	5.44	4.89	4.94	4.59	6.04	1.10	0.88	0.86	0.96	0.95	1.02	0.78
	3.4	NWC	32258	22	27.8	5.1058	0	7.08	5.53	6.96	7.02	7.15	6.96	6.87	8.25	1.28	1.02	1.01	0.99	1.02	1.03	0.86
	3.5	NWC	32258	22	27.8	7.1891	0	7.94	5.53	6.96	8.33	8.36	6.96	8.35	8.70	1.44	1.14	0.95	0.95	1.14	0.95	0.91
	4.1	NWC	32258	22	28.0	2.0005	0	4.85	2.80	5.56	4.40	4.67	4.60	4.40	6.41	1.73	0.87	1.10	1.04	1.05	1.10	0.76
	4.2	NWC	32258	22	28.0	4.0009	0	6.75	5.54	7.01	6.22	6.42	6.43	6.00	7.82	1.22	0.96	1.09	1.05	1.05	1.12	0.86
	4.3	NWC	32258	22	29.9	6.0014	0	8.13	5.69	7.48	7.61	8.07	7.48	7.79	9.01	1.43	1.09	1.07	1.01	1.09	1.04	0.90
	4.4	NWC	32258	22	29.9	8.0018	0	9.65	5.69	7.48	8.79	9.23	7.48	8.97	9.35	1.69	1.29	1.10	1.05	1.29	1.08	1.03
	4.5	NWC	32258	22	30.2	10.0023	0	9.09	5.72	7.56	9.83	10.33	7.56	9.07	9.37	1.59	1.20	0.93	0.88	1.20	1.00	0.97
	5.1	NWC	32258	22	16.9	1.5344	0	3.51	2.15	4.22	3.85	3.27	3.15	2.92	4.26	1.64	0.83	0.91	1.07	1.11	1.21	0.82
	5.2	NWC	32258	22	18.1	3.0688	0	4.82	3.61	4.51	5.44	4.46	4.51	4.26	5.33	1.34	1.07	0.89	1.08	1.07	1.13	0.90
	5.3	NWC	32258	22	16.4	4.6032	0	5.58	3.29	4.11	6.67	4.96	4.11	4.93	5.19	1.70	1.36	0.84	1.12	1.36	1.13	1.07
	5.4	NWC	32258	22	17.8	6.1376	0	5.48	3.56	4.44	7.70	5.83	4.44	5.33	5.50	1.54	1.23	0.71	0.94	1.23	1.03	1.00
Mattock (1976)	A1	NWC	32258	19	41.5	1.5628	0	5.24	2.19	4.94	3.89	5.02	4.98	3.52	7.49	2.39	1.06	1.35	1.04	1.05	1.49	0.70
	A2	NWC	32258	19	41.5	3.1257	0	5.51	4.38	7.13	5.49	7.18	6.94	6.65	9.30	1.26	0.77	1.00	0.77	0.79	0.83	0.59
	A3	NWC	32258	19	40.1	5.0344	0	7.92	6.51	9.80	6.97	8.98	8.61	8.04	10.58	1.22	0.81	1.14	0.88	0.92	0.99	0.75
	A4	NWC	32258	19	40.5	6.7126	0	9.78	6.54	10.13	8.05	10.48	9.97	9.42	11.54	1.50	0.97	1.21	0.93	0.98	1.04	0.85
	A5	NWC	32258	19	42.2	7.7582	0	10.34	6.68	10.34	8.66	11.62	10.55	10.43	12.30	1.55	1.00	1.19	0.89	0.98	0.99	0.84
	A6	NWC	32258	19	40.7	10.3846	0	12.13	6.55	10.16	10.02	13.14	10.16	12.20	12.56	1.85	1.19	1.21	0.92	1.19	0.99	0.97
	A6A	NWC	32258	19	41.1	10.3846	0	12.82	6.59	10.28	10.02	13.26	10.28	12.34	12.69	1.94	1.25	1.28	0.97	1.25	1.04	1.01
	A7	NWC	32258	19	41.1	13.0348	0	13.37	6.59	10.28	11.22	14.90	10.28	12.34	12.73	2.03	1.30	1.19	0.90	1.30	1.08	1.05
Mattock and Hawkins (1972)	9.2	NWC	32258	25	37.9	6.7948	-10.2	17.64	6.33	9.47	8.10	10.06	9.47	11.37	13.72	2.79	1.86	2.18	1.75	1.86	1.55	1.29
	9.3	NWC	32258	25	27.1	6.8078	-2.8	10.44	5.43	6.79	8.11	8.02	6.79	8.14	10.04	1.92	1.54	1.29	1.30	1.54	1.28	1.04
	9.4	NWC	32258	25	27.1	6.9900	0	9.57	5.43	6.79	8.22	8.11	6.79	8.14	8.43	1.76	1.41	1.16	1.18	1.41	1.18	1.13
	9.5	NWC	32258	25	44.4	4.4257	-11.4	19.77	5.37	10.34	6.54	8.97	8.50	13.31	15.45	3.69	1.91	3.02	2.20	2.33	1.49	1.28
	9.6	NWC	32258	25	44.4	2.2129	-11.0	19.09	2.68	10.34	4.62	6.22	6.08	13.31	14.62	7.11	1.85	4.13	3.07	3.14	1.43	1.31
Mattock at el. (1976)	A0	sand-LWC	32258	9.5	29.1	0.0000	0	3.45	0.00	1.65	0.00	0.00	0.87	0.00	2.77	-	2.08	-	-	3.96	-	1.24
	A1	sand-LWC	32258	9.5	25.8	1.4469	0	5.22	1.72	3.10	3.18	3.87	3.22	2.86	5.21	3.03	1.68	1.64	1.35	1.62	1.83	1.00
	A2	sand-LWC	32258	9.5	28.2	3.2521	0	6.30	3.87	4.91	4.76	5.86	4.96	4.30	7.23	1.63	1.28	1.32	1.08	1.27	1.46	0.87
	A3	sand-LWC	32258	9.5	26.9	4.8368	0	7.03	5.39	6.49	5.81	6.83	5.88	5.57	7.94	1.30	1.08	1.21	1.03	1.19	1.26	0.88
	A4	sand-LWC	32258	9.5	28.2	6.1734	0	7.58	5.50	6.89	6.56	7.87	6.79	6.64	8.68	1.38	1.10	1.15	0.96	1.12	1.14	0.87
	A5	sand-LWC	32258	9.5	27.3	7.7168	0	8.20	5.46	6.82	7.34	8.51	6.82	7.87	8.70	1.50	1.20	1.12	0.96	1.20	1.04	0.94

	A6	sand-LWC	32258	9.5	29.3	9.4255	0	9.26	5.50	6.89	8.11	9.81	7.32	8.78	9.33	1.68	1.34	1.14	0.94	1.26	1.05	0.99
	E0	all-LWC	32258	9.5	27.3	0.0000	0	3.86	0.00	1.65	0.00	0.00	0.74	0.00	2.57	-	2.33	-	-	5.19	-	1.50
	E1	all-LWC	32258	9.5	28.6	1.5847	0	5.37	1.66	3.24	2.93	4.24	3.12	2.67	5.63	3.23	1.66	1.83	1.27	1.72	2.01	0.95
	E2	all-LWC	32258	9.5	27.8	3.1694	0	6.01	3.33	4.82	4.15	5.74	4.29	3.94	7.00	1.81	1.25	1.45	1.05	1.40	1.53	0.86
	E3	all-LWC	32258	9.5	28.0	4.7541	0	6.61	4.99	6.41	5.08	6.94	5.25	5.20	7.98	1.33	1.03	1.30	0.95	1.26	1.27	0.83
	E4	all-LWC	32258	9.5	27.83	6.4490	0	7.92	5.50	6.89	5.92	7.95	6.08	6.56	8.51	1.44	1.15	1.34	1.00	1.30	1.21	0.93
	E5	all-LWC	32258	9.5	28.4	7.6548	0	8.27	5.50	6.89	6.45	8.71	6.67	7.52	8.85	1.50	1.20	1.28	0.95	1.24	1.10	0.93
	E6	all-LWC	32258	9.5	27.9	9.5151	0	8.61	5.50	6.89	7.19	9.52	6.98	8.37	8.60	1.57	1.25	1.20	0.90	1.23	1.03	1.00
	G0	all-LWC	32258	12.7	27.8	0.0000	0	3.65	0.00	1.65	0.00	0.00	0.75	0.00	2.90	-	2.21	-	-	4.87	-	1.26
	G1	all-LWC	32258	12.7	28.6	1.5847	0	5.65	1.66	3.24	2.93	4.23	3.12	2.67	5.71	3.40	1.74	1.93	1.33	1.81	2.12	0.99
	G2	all-LWC	32258	12.7	26.7	3.0592	0	5.83	3.21	4.71	4.08	5.53	4.14	3.85	6.80	1.81	1.24	1.43	1.05	1.41	1.52	0.86
	G3	all-LWC	32258	12.7	28.2	4.7128	0	7.30	4.95	6.37	5.06	6.95	5.25	5.17	7.99	1.48	1.15	1.44	1.05	1.39	1.41	0.91
	G4	all-LWC	32258	12.7	30.5	6.4490	0	7.92	5.50	6.89	5.92	8.44	6.36	6.56	9.05	1.44	1.15	1.34	0.94	1.25	1.21	0.88
	G5	all-LWC	32258	12.7	27.6	7.8546	0	7.85	5.50	6.89	6.53	8.65	6.67	7.68	8.58	1.43	1.14	1.20	0.91	1.18	1.02	0.92
	G6	all-LWC	32258	12.7	27.6	9.4255	0	8.20	5.50	6.89	7.16	9.40	6.90	8.28	8.48	1.49	1.19	1.15	0.87	1.19	0.99	0.97
	M0	NWC	32258	12.7	27.1	0.0000	0	4.07	0.00	2.76	0.00	0.00	0.99	0.00	2.97	-	1.48	-	-	4.11	-	1.37
	M1	NWC	32258	12.7	28.8	1.5434	0	5.24	2.16	4.92	3.86	4.20	4.13	3.47	5.89	2.42	1.07	1.36	1.25	1.27	1.51	0.89
	M2	NWC	32258	12.7	26.9	3.1970	0	6.75	4.48	6.72	5.56	5.65	5.65	5.24	7.18	1.51	1.01	1.22	1.19	1.20	1.29	0.94
	M3	NWC	32258	12.7	27.5	4.7541	0	7.65	5.50	6.88	6.78	6.87	6.88	6.56	8.21	1.39	1.11	1.13	1.11	1.11	1.17	0.93
	M4	NWC	32258	12.7	28.6	6.1734	0	7.85	5.59	7.15	7.72	7.93	7.15	7.80	8.97	1.41	1.10	1.02	0.99	1.10	1.01	0.88
	M5	NWC	32258	12.7	27.1	7.9924	0	8.82	5.42	6.78	8.79	8.61	6.78	8.13	8.88	1.63	1.30	1.00	1.02	1.30	1.08	0.99
	M6	NWC	32258	12.7	28.4	9.5909	0	9.09	5.57	7.10	9.63	9.67	7.10	8.52	9.25	1.63	1.28	0.94	0.94	1.28	1.07	0.98
Mattock at el. (1975)	E1U	NWC	54193	19	28.0	3.7974	0	7.50	5.32	6.99	6.06	6.26	6.26	5.84	7.70	1.41	1.07	1.24	1.20	1.20	1.29	0.97
	E4U	NWC	54193	19	26.6	3.5380	1.4	6.52	4.95	5.78	5.85	5.88	5.90	4.39	6.31	1.32	1.13	1.11	1.11	1.10	1.49	1.03
	E6U	NWC	54193	19	28.4	3.6605	2.8	4.18	5.12	4.02	5.95	6.21	6.20	2.04	5.12	0.82	1.04	0.70	0.67	0.67	2.05	0.82
	F1U	NWC	54193	19	27.8	5.6421	0	9.43	5.52	6.95	7.38	7.47	6.95	7.29	8.45	1.71	1.36	1.28	1.26	1.36	1.29	1.12
	F4U	NWC	54193	19	28.8	5.7502	1.4	7.88	5.60	7.19	7.45	7.71	7.19	6.37	8.16	1.41	1.10	1.06	1.02	1.10	1.24	0.97
	F6U	NWC	54193	19	29.2	5.5124	2.8	7.34	5.64	6.61	7.30	7.64	7.31	5.13	7.22	1.30	1.11	1.01	0.96	1.00	1.43	1.02
Yang et al. (2012)	A4	all-LWC	24000	4	31.2	0.0000	0	1.77	0.00	1.65	0.00	0.00	0.79	0.00	2.05	-	1.07	-	-	2.22	-	0.86
	A8	all-LWC	24000	8	36.2	0.0000	0	2.63	0.00	1.65	0.00	0.00	0.86	0.00	2.88	-	1.59	-	-	3.08	-	0.91
	A13	all-LWC	24000	13	31.8	0.0000	0	2.54	0.00	1.65	0.00	0.00	0.80	0.00	3.13	-	1.54	-	-	3.17	-	0.81
	A19	all-LWC	24000	19	37.4	0.0000	0	3.06	0.00	1.65	0.00	0.00	0.87	0.00	3.92	-	1.85	-	-	3.51	-	0.78
	S4	sand-LWC	24000	4	34.8	0.0000	0	1.92	0.00	1.65	0.00	0.00	0.95	0.00	2.35	-	1.16	-	-	2.02	-	0.82

	S8	sand-LWC	24000	8	29.9	0.0000	0	2.55	0.00	1.65	0.00	0.00	0.88	0.00	2.63	-	1.54	-	-	2.89	-	0.97
	S13	sand-LWC	24000	13	36.0	0.0000	0	2.84	0.00	1.65	0.00	0.00	0.97	0.00	3.52	-	1.72	-	-	2.93	-	0.81
	S19	sand-LWC	24000	19	33.0	0.0000	0	3.19	0.00	1.65	0.00	0.00	0.93	0.00	3.73	-	1.93	-	-	3.45	-	0.85
	N4	NWC	24000	4	25.8	0.0000	0	1.70	0.00	2.76	0.00	0.00	0.96	0.00	1.90	-	0.62	-	-	1.76	-	0.89
	N8	NWC	24000	8	29.6	0.0000	0	2.79	0.00	2.76	0.00	0.00	1.03	0.00	2.68	-	1.01	-	-	2.70	-	1.04
	N13	NWC	24000	13	27.4	0.0000	0	3.01	0.00	2.76	0.00	0.00	0.99	0.00	2.98	-	1.09	-	-	3.03	-	1.01
	N19	NWC	24000	19	36.2	0.0000	0	3.89	0.00	2.76	0.00	0.00	1.14	0.00	4.15	-	1.41	-	-	3.41	-	0.94
Hwang and Yang (2016)	NH-N-0	NWC	31500	25	62.5	0.0000	0	5.75	0.00	2.76	0.00	0.00	1.50	0.00	6.73	-	2.09	-	-	3.83	-	0.85
	NH-V-0	NWC	31500	25	62.5	4.2499	0	10.81	5.95	8.71	6.41	10.97	9.89	8.91	13.25	1.82	1.24	1.69	0.99	1.09	1.21	0.82
	NH-X-0	NWC	31500	25	62.5	3.0234	0	12.88	2.97	6.96	5.39	8.95	8.36	6.76	14.89	4.33	1.85	2.39	1.44	1.54	1.90	0.87
	NH-N-0.15	NWC	31500	25	62.5	0.0000	9.4	16.4	0.00	10.34	0.00	0.00	1.50	13.01	16.87	-	1.59	-	-	10.73	1.26	0.97
	NH-V-0.15	NWC	31500	25	62.5	4.2499	9.4	21.1	5.95	10.34	6.41	10.97	9.89	16.41	18.31	3.55	2.04	3.29	1.92	2.13	1.29	1.15
	NH-X-0.15	NWC	31500	25	62.5	3.0234	9.4	23.01	2.97	10.34	5.39	8.95	8.36	15.42	21.01	7.73	2.23	4.27	2.57	2.75	1.49	1.10
	NN-N-0.15	NWC	31500	25	29.8	0.0000	4.5	11.54	0.00	7.45	0.00	0.00	1.04	6.56	8.38	-	1.55	-	-	11.14	1.76	1.38
	NN-V-0.15	NWC	31500	25	29.8	4.2499	4.5	14.63	5.68	7.45	16.60	6.85	6.83	8.94	9.24	2.57	1.96	0.88	2.14	2.14	1.64	1.58
	NN-X-0.15	NWC	31500	25	29.8	3.0234	4.5	14.24	2.97	7.45	14.68	5.83	5.77	8.94	12.21	4.79	1.91	0.97	2.44	2.47	1.59	1.17
	HH-N-0	HWC	31500	25	58.8	0.0000	0	8.99	0.00	2.76	0.00	0.00	1.45	0.00	6.78	-	3.26	-	-	6.18	-	1.33
	HH-V-0	HWC	31500	25	58.8	4.2499	0	14.23	5.95	8.71	6.41	10.53	9.60	8.91	13.29	2.39	1.63	2.22	1.35	1.48	1.60	1.07
	HH-X-0	HWC	31500	25	58.8	3.0234	0	13.83	2.97	6.96	5.40	8.66	8.13	6.76	14.92	4.65	1.99	2.56	1.60	1.70	2.05	0.93

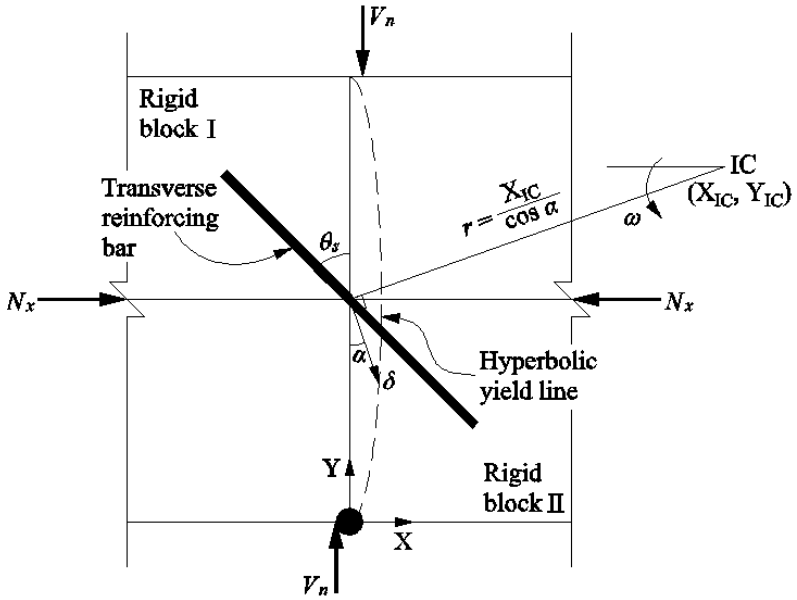

Fig. 1 – Idealized failure mechanism of a monolithic concrete interface.

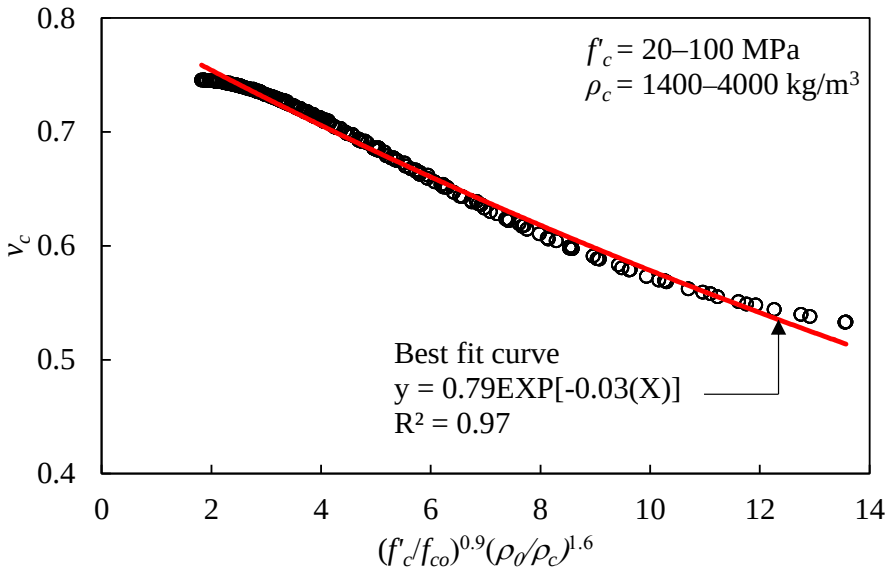

Fig. 2 – Modeling of ν_c for different concretes.

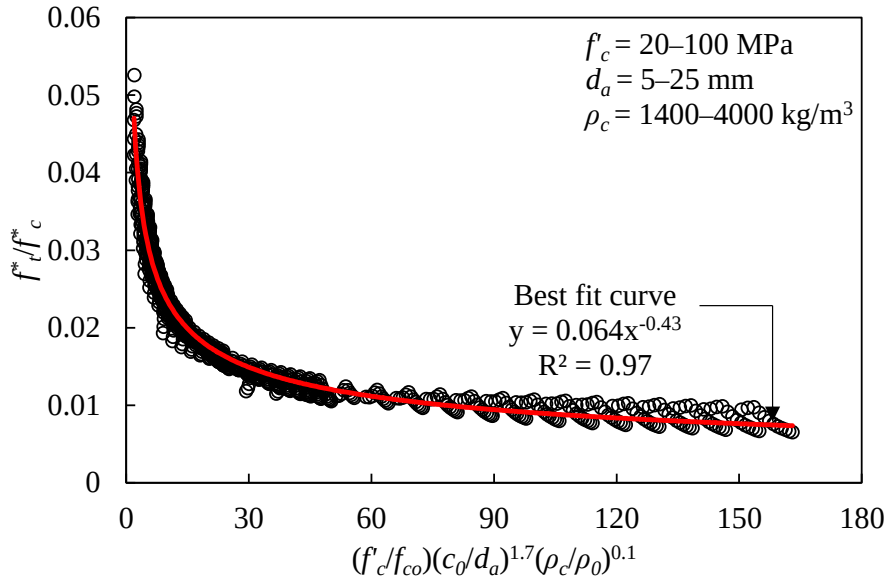

Fig. 3 – Modeling of f_t^* / f_c^* for different concretes.

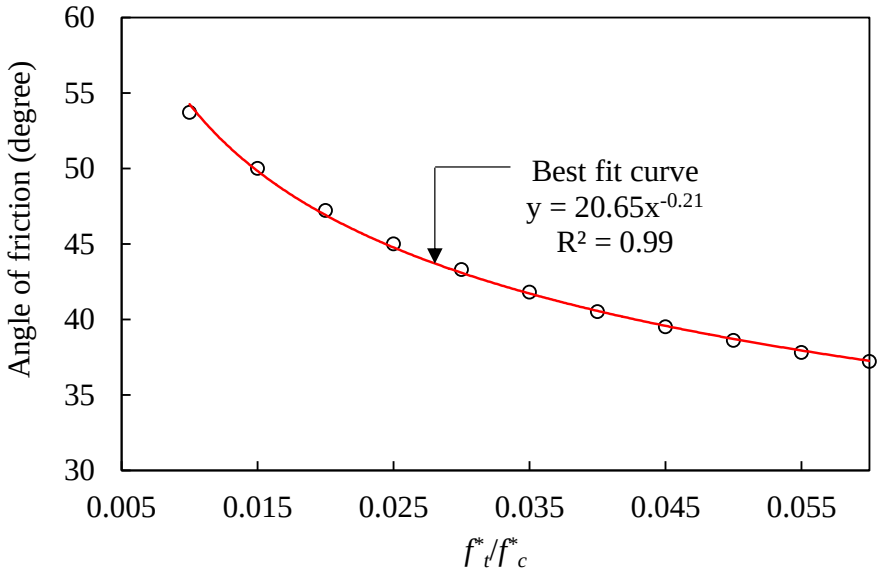

Fig. 4 – Variation of φ against f_t^* / f_c^*.

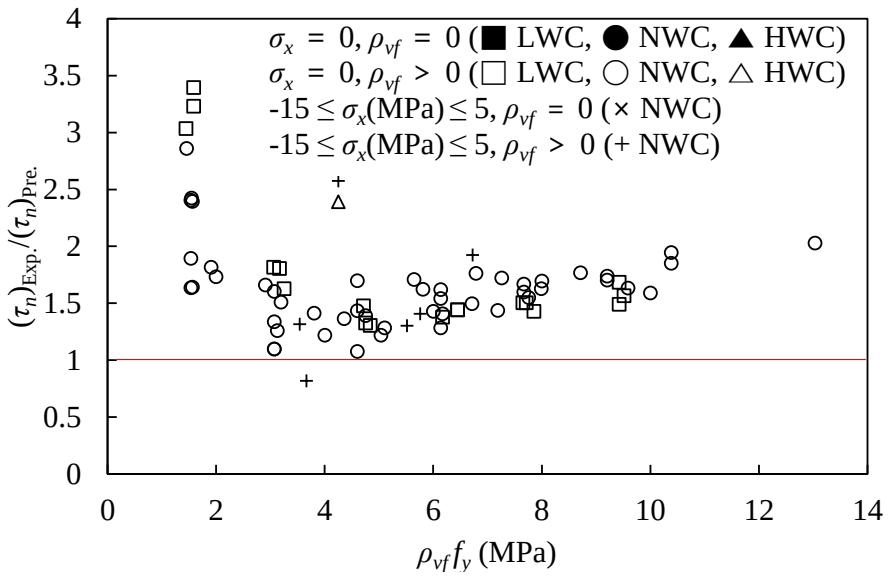

(a) ACI 318-11

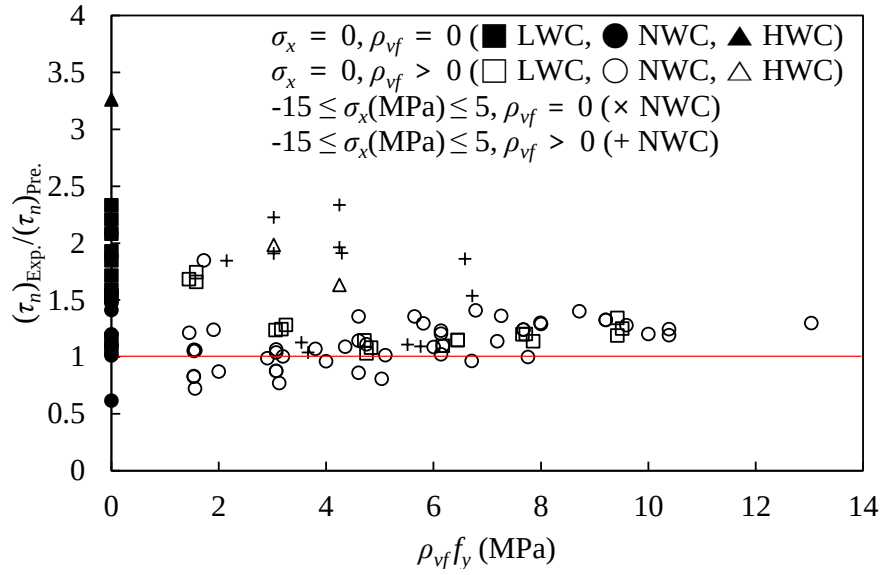

(b) AASHTO

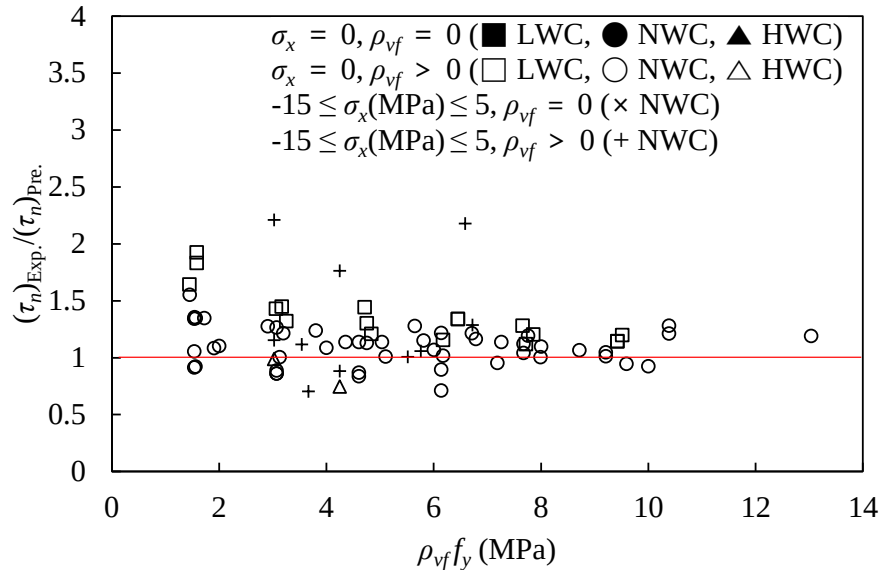

(c) Shaikh

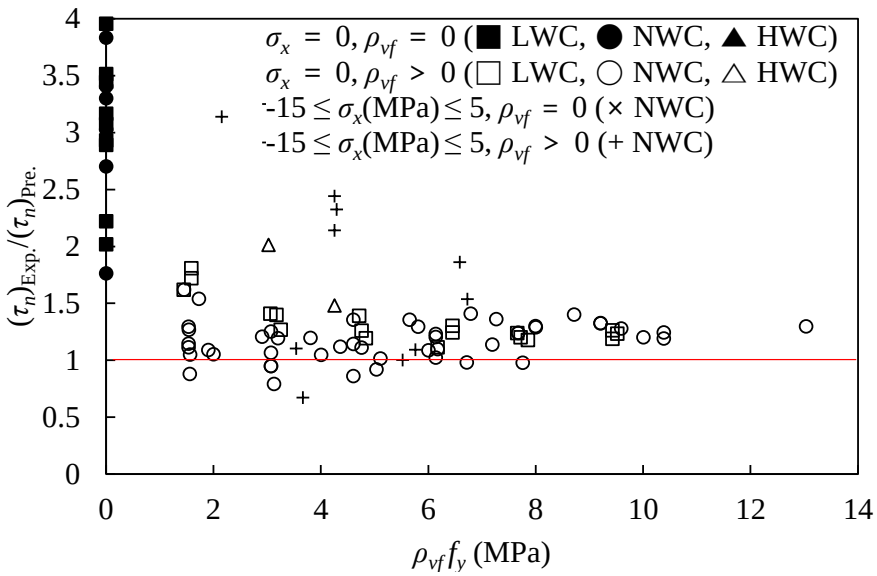

(d) Loov and Patnaik

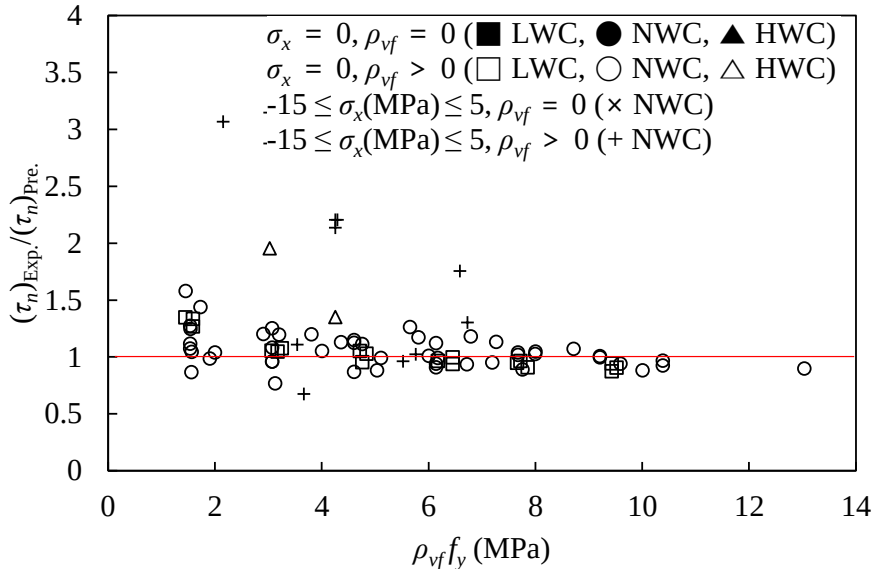

(e) Walraven et al.

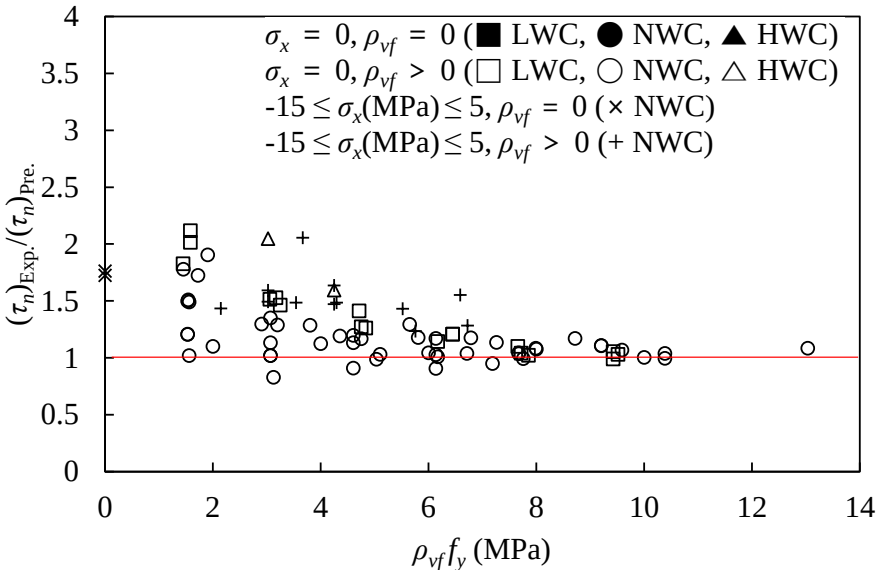

(f) Mattock

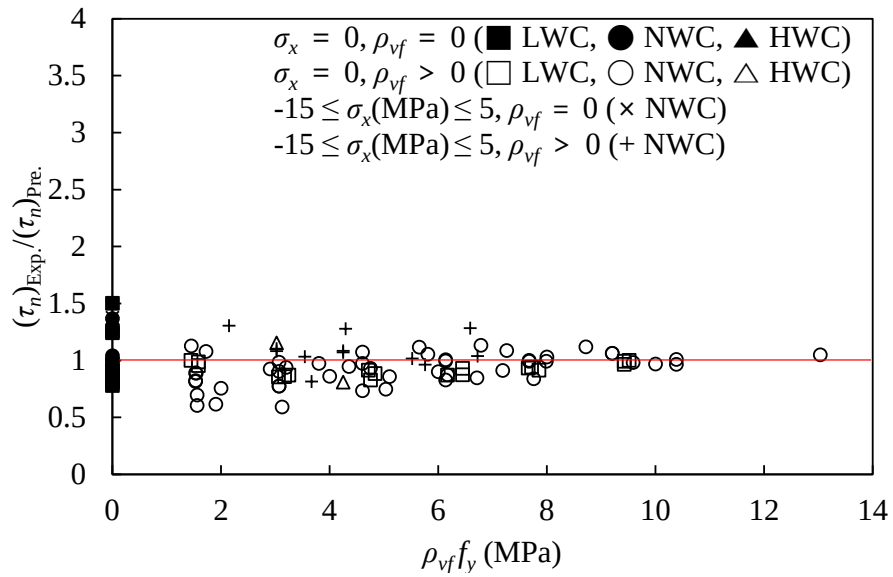

(g) This study

Fig. 5 – Comparisons of measured and predicted shear friction capacities.

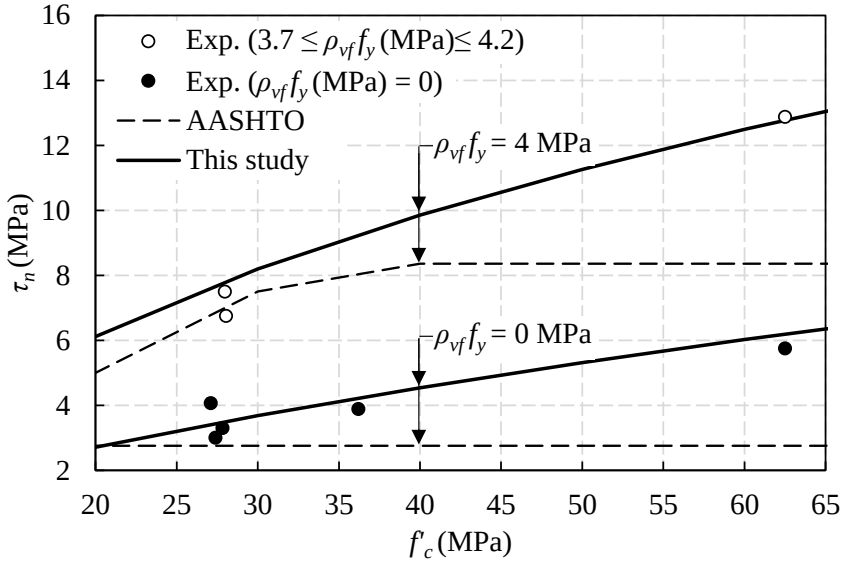

(a) Compressive strength of NWC

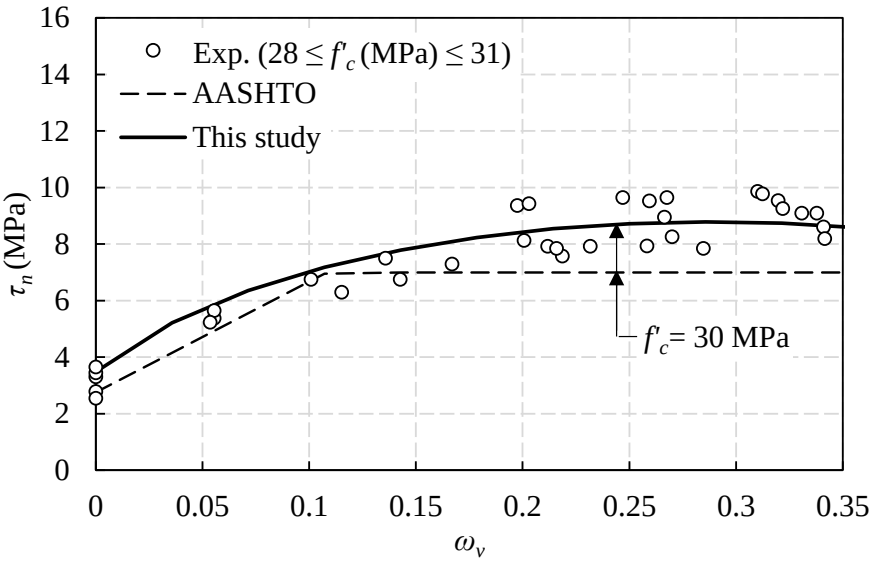

(b) Transverse reinforcement

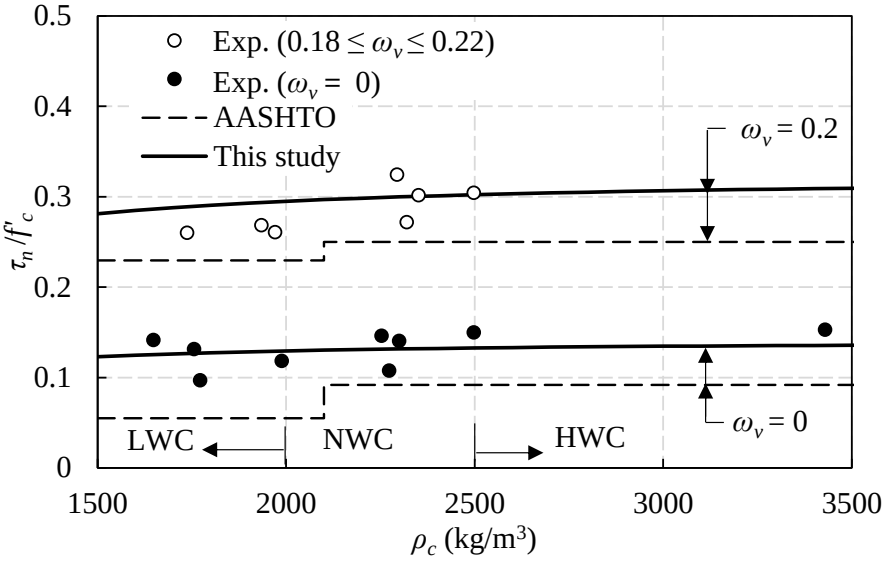

(c) Unit weight of concrete

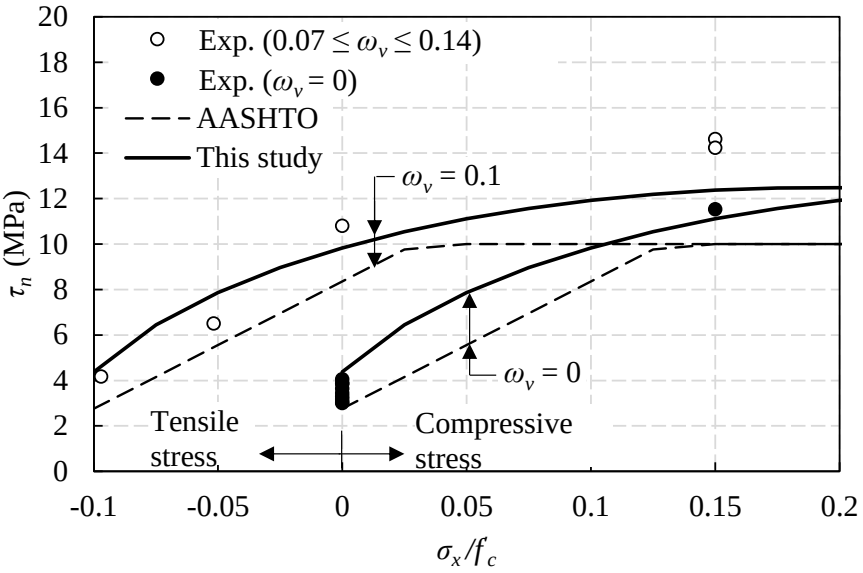

(d) Additional axial stresses

Fig. 6 – Effect of different parameters on shear friction strength.